hep-ph/9503266
DTP/95/22
March 1995

The gluon distribution at small x obtained from a unified evolution equation

J. Kwieciński[1] and A. D. Martin,

Department of Physics, University of Durham, Durham, DH1 3LE, England
and
P. J. Sutton,

Department of Physics, University of Manchester, Manchester, M13 9PL, England

Abstract

We solve a unified integral equation to obtain the x, Q_T and Q dependence of the gluon distribution of a proton in the small x regime; where x and Q_T are the longitudinal momentum fraction and the transverse momentum of the gluon probed at a scale Q. The equation generates a gluon with a steep $x^{-\lambda}$ behaviour, with $\lambda \sim 0.5$, and a Q_T distribution which broadens as x decreases. We compare our solutions with, on the one hand, those that we obtain using the double-leading-logarithm approximation to Altarelli-Parisi evolution and, on the other hand, to those that we determine from the BFKL equation.

[1]On leave from Henryk Niewodniczański Institute of Nuclear Physics, 31-342 Kraków, Poland.

1. Introduction

Understanding the details of the small x behaviour of parton distributions is one of the most challenging problems of perturbative QCD [1, 2]. Moreover this topic has recently become of particular phenomenological interest with the advent of measurements of deep inelastic scattering at the high energy electron-proton collider, HERA, which have opened up the small x regime [3]. There now exist data for the proton structure function F_2 for x as low as $x \sim 10^{-4}$. These measurements reveal a significant rise of F_2 with decreasing x, which has been taken to signal novel phenomena, although whether, in fact, this is the case or whether conventional explanations suffice, remains to be settled.

First we recall the conventional treatment of "hard" scattering processes involving hadrons at moderate values of x, say $x \gtrsim 0.05$. Then the observable quantities are calculated in perturbative QCD using the mass factorization theorem [4] in which the collinear singularities, which occur in the partonic subprocesses, are absorbed into universal parton densities. To be specific let us take as an example the longitudinal structure function[2] of the proton $F_L(x, Q^2)$ and, for simplicity, consider only the gluon[3] partonic constituent. Then we have

$$F_L(x, Q^2) = \int_x^1 \frac{dx'}{x'} g(x', Q^2) \hat{F}_L(x/x', \alpha_S(Q^2)) \tag{1}$$

where we have chosen the mass factorization scale to be the "hard" scale Q^2 of the process. The absorption of the collinear logarithmic singularities make the gluon density $g(x, Q^2)$ "run", with a Q^2 dependence given by the Altarelli-Parisi evolution equations [5]. That is perturbative QCD does not determine the gluon absolutely but only its evolution from a non-perturbative input form. Altarelli-Parisi evolution resums the leading $\alpha_S \log(Q^2/Q_0^2)$ contributions. In a physical gauge the $\alpha_S^n \log^n(Q^2/Q_0^2)$ contribution can be associated with a space-like chain of n gluon emissions in which the successive gluon transverse momenta are strongly ordered along the chain [6], that is $k_{T1}^2 \ll \ldots \ll k_{Tn}^2 \ll Q^2$. The next-to-leading order contribution corresponds to the case when a pair of gluons are emitted without strong k_T-ordering (and iterations of this configuration). Then we have a power of α_S unaccompanied by $\log(Q^2/Q_0^2)$. A key feature of this conventional partonic approach is that the gluonic structure function, $\hat{F}_L$ (which at lowest order arises from the subprocess $\gamma^* g \to q\overline{q}$) is calculated assuming that the incoming gluon has negligible transverse momentum (and hence virtuality) as compared to the scale of the hard process. That is, on account of strong-ordering, we are able to work in terms of the density $g(x, Q^2)$ of the gluon integrated over its transverse momentum Q_T.

At sufficiently high electron-proton c.m. energy, $\sqrt{s}$, we encounter a second large variable, $1/x \sim s/Q^2$, and in this small x regime we must resum the leading $\alpha_S \log(1/x)$ contributions.

[2]We choose F_L as our example, rather than F_2, because we are interested in hard scattering observables which are driven directly by the gluon. We could have used F_2 but then we would have to deal with the collinear singularities of $\hat{F}_2$ associated with the $g \to q\overline{q}$ transition. These singularities are absorbed into the universal sea quark distributions. The simplification in which we neglect the sea quarks would therefore have been incomplete, even at leading order, and we would have had to broaden the discussion.

[3]The gluon dominates the other partons in the small x regime, which is the main concern of our study.

The key ingredients of the QCD framework in this regime are the high-energy Q_T-factorization theorem [7] and the BFKL equation [8, 9] for the gluon distribution, $F(x, Q_T)$, unintegrated over its transverse momentum Q_T. Using Q_T-factorization our sample observable is now given by

$$F_L(x, Q^2) = \int_x^1 \frac{dx'}{x'} \int \frac{d^2Q_T}{\pi} F(x', Q_T) \tilde{F}_L\Big(\frac{x}{x'}, \frac{Q_T^2}{Q^2}, \alpha_S(Q^2)\Big) \tag{2}$$

where $\tilde{F}_L$ denotes the gluonic structure function calculated using an off-shell ($Q_T^2 \neq 0$) gluon. If we were to return to the strongly-ordered transverse momentum configuration then

$$\tilde{F}_L \to \hat{F}_L = \tilde{F}_L(x/x', 0, \alpha_S(Q^2)) \tag{3}$$

and

$$xg(x, Q^2) = \int \frac{d^2Q_T}{\pi} F(x, Q_T) \Theta(Q - Q_T), \tag{4}$$

though, of course, it is inappropriate to work in terms of the familiar integrated distribution $g(x, Q^2)$ at small x.

The BFKL equation for the unintegrated gluon density $F(x, Q_T)$ sums the leading $\alpha_S \log(1/x)$ contributions. The strong-ordering in transverse momenta is no longer applicable and we now have a "random walk" or diffusion in k_T as we proceed along the chain. The enlarged k_T phase space leads to a $x^{-\lambda}$ growth, with decreasing x, where $\lambda \sim 0.5$. Indeed the observed behaviour of F_2 appears consistent with the precocious onset of this leading $\log(1/x)$ behaviour of the gluon [10], but the definitive confirmation that this is the case must await the calculation of the subleading corrections to the BFKL equation. Clearly the BFKL equation, which resums the leading $\log(1/x)$ contributions, has a limited region of validity. In principle, it is restricted to the region $\alpha_S \log(1/x) \sim \mathcal{O}(1)$ and $\alpha_S \log(Q^2/Q_0^2) \ll 1$, where Q_0^2 indicates the boundary of the non-perturbative domain, $Q_0^2 \sim 1$ GeV^2. To make progress we need to know how the BFKL formalism links with the conventional Altarelli-Parisi dynamics at larger x and large $\log(Q^2/Q_0^2)$.

A theoretical framework which gives a unified treatment throughout the x, Q^2 kinematic region has been provided by Catani, Ciafaloni, Fiorani and Marchesini [11-15]. The resulting equation, which we shall call the CCFM equation, treats both the small and large x regions in a unified way. The equation is based on the coherent radiation of gluons, which leads to an angular ordering of the gluon emissions along the chain. In the leading $\log(1/x)$ approximation the CCFM equation reduces to the BFKL equation, whereas at moderate x the angular ordering becomes an ordering in the gluon transverse momenta and the CCFM equation becomes equivalent to standard Altarelli-Parisi evolution [5]. The angular ordering introduces an additional scale (which turns out to be essentially the hard scale Q of the probe), which is needed to specify the maximum angle of gluon emission. Thus we must work with a scale-dependent, unintegrated gluon density $F(x, Q_T, Q)$. At very small x the angular ordering does not provide any constraint on the transverse momenta along the chain and F becomes the Q-independent gluon of the BFKL equation.

The aim of our paper is to study the CCFM equation in detail and, in particular, to obtain numerical solutions so as to reveal the small x behaviour of the gluon distribution in the proton. In Section 2 we sketch the derivation of the CCFM equation, while in Section 3 we study its properties in the important small x region. We make approximations which both simplify the discussion and facilitate the solution of the equation. To gain insight we study both the "folded" and "unfolded" versions of the equation. In Section 4 we present numerical solutions $F(x, Q_T, Q)$ of the CCFM equation and compare them with solutions that we obtain from solving the two limiting versions of the equation. That is we compare the CCFM solutions with those obtained from (i) the double-leading-logarithm approximation to the Altarelli-Parisi equation and (ii) the BFKL equation. Section 5 contains our conclusions on the small x behaviour of the gluon.

2. Coherent branching : the master equation for the gluon

The perturbative evaluation of physical QCD quantities in general, and parton distributions in particular, is complicated by the presence of large logarithms which arise from the emission of both soft and collinear gluons. The origin of the large logarithms can be seen from Fig. 1. The differential probability for emitting a gluon of 4-momentum q is of the form

$$dP \sim \alpha_S \frac{dz_g}{z_g} \frac{dq_T^2}{q_T^2} \tag{5}$$

where q_T is the transverse momentum and z_g is the longitudinal momentum expressed as a fraction of the momentum of the parent gluon.

Here we focus attention on the gluon distribution within a proton. To predict the correct behaviour of the distribution it is necessary to resum the large logarithms which arise not just from single but from multigluon emissions to all orders in α_S. A typical contribution is shown in Fig. 2, where a gluon of low space-like virtuality evolves to higher virtuality and lower energy by successive gluon emission. It can be shown that the emissions are coherent in the sense that there is angular ordering, $\theta_i > \theta_{i-1}$, along the chain, where θ_i is the angle that the i^{th} gluon makes to the original direction [11-16]. Outside this region there is destructive interference such that the multigluon contributions vanish to leading order. We speak of coherent branching.

As mentioned in Section 1, due to the presence of angular (rather than transverse momentum) ordering of the emitted gluons we need to expose the transverse momentum, Q_T, dependence of the probed gluon. That is we work in terms of the scale (Q) dependent "unintegrated" gluon density $F(x, Q_T, Q)$, which specifies the chance of finding a gluon with longitudinal momentum fraction x and transverse momentum of magnitude Q_T [13]. The integral equation for $F(x, Q_T, Q)$, which effects the summation of the large logarithms, can be approximated on the one hand, to yield the BFKL equation at small x, where F becomes independent of Q and, on the other hand, to yield at moderate x the Altarelli-Parisi (or GLAP) evolution equation for the integrated distribution $g(x, Q^2)$. It is this master equation which we wish to investigate and to solve.

It is necessary to outline the derivation of the equation [11, 12, 13]. A crucial development has been the proof of the soft gluon factorization theorems which allow the inclusion, not only real gluon emission, but also the virtual emission contributions which tame the singular behaviour in the two boundary regions $z \to 0$ and $z \to 1$. A recurrence relation can then be obtained which expresses the contribution from n-gluon emission in terms of that from $n-1$ emission. In essence, we integrate the differential probability dP for the emission of the extra gluon over the relevant region of phase space, where (5) takes the explicit form

$$dP = \Delta_S \tilde{P} dz \frac{dq_T^2}{q_T^2} \Theta(\theta - \theta'). \tag{6}$$

Here $\Theta(\theta - \theta')$ reflects the angular ordering and $\tilde{P}$ is the gluon-gluon splitting function

$$\tilde{P} = \overline{\alpha}_S \left[\frac{1}{1-z} + \Delta_{NS} \frac{1}{z} - 2 + z(1-z) \right]. \tag{7}$$

We define $\overline{\alpha}_S = C_A \alpha_S / \pi = 3\alpha_S/\pi$. The multiplicative factors Δ_S and Δ_{NS}, known as the Sudakov and non-Sudakov form factors, arise from the resummation of the virtual corrections. They cancel the singularities manifest as $z \to 1$ and $z \to 0$ respectively. These form factors have exponential forms which we present in eqs. (10) and (11) below.

We use (6) to obtain a recursion relation expressing the distribution $\mathcal{F}_n$ in terms of $\mathcal{F}_{n-1}$. The distribution $\mathcal{F}_n(x, Q_T, z, q)$ corresponds to the n-rung ladder diagram, where the variables are defined in Fig. 3. Following refs. [13, 16] we impose the angular-ordered constraint by introducing rescaled transverse momenta

$$q \equiv \frac{q_T}{1-z} \approx \theta E', \quad q' \equiv \frac{q'_T}{1-z'} \approx \theta' E'' \tag{8}$$

where $1-z$ is the longitudinal momentum fraction of the gluon emitted at angle θ and E' is the energy component of the exchanged gluon with spacelike momentum $x'p$. Here we have used the small angle approximation, $\tan\theta \approx \theta$. The coherence constraint $\theta > \theta'$ therefore implies $q > z'q'$ and so (6) gives

$$\mathcal{F}_n(x, Q_T, z, q) = \int_{x/z}^1 dz' \int \frac{d^2q'}{\pi q'^2} \Theta(q - z'q') \Delta_S(q, z'q') \tilde{P}(z, q, Q_T) \mathcal{F}_{n-1}\left(\frac{x}{z}, Q'_T, z', q'\right), \tag{9}$$

see Fig. 3. Due to the presence of angular ordering, it appears that we have to consider a less inclusive structure function than the unintegrated distribution $F(x, Q_T, Q)$ itself. To be precise we have exposed not only the x, Q_T of the probed gluon, but also the z, q dependence which specifies the previous emitted gluon. Note that the variable Q'_T in $\mathcal{F}_{n-1}$ is the magnitude of the vector sum $\boldsymbol{Q}_T + (1-z)\boldsymbol{q}$ and, so, in principle, the angular integration in d^2q' is non-trivial.

The Sudakov form factor is given by

$$\Delta_S(q, z'q') = \exp\left(- \int_{(z'q')^2}^{q^2} \frac{dk^2}{k^2} \int_0^1 dx \frac{\overline{\alpha}_S}{1-z} \right). \tag{10}$$

The region of integration corresponds to the angular-ordered region from the angle θ' of emission of the $(n-1)^{th}$ gluon to θ of the n^{th} gluon. Indeed Δ_S can be interpreted as the probability for not emitting a gluon in this angular region. This observation is consistent with (6) which gives the differential probability for **single** gluon emission in an element of phase space specified by z, q_T^2; the factor Δ_S ensuring that there is no prior emission.

The splitting function $\tilde{P}(z, q, Q_T)$ is given by (7) in which the $1/z$ singularity is screened by virtual corrections contained in the non-Sudakov form factor

$$\begin{aligned} \Delta_{NS}(z, q, Q_T) &= \exp\left(-\overline{\alpha}_S \int_z^{z_0} \frac{dz'}{z'} \int \frac{dk^2}{k^2} \Theta(Q_T^2 - k^2)\Theta(k - z'q)\right) \quad (11) \\ &= \exp\left(-\overline{\alpha}_S \log\left(\frac{z_0}{z}\right) \log\left(\frac{Q_T^2}{z_0 z q^2}\right)\right), \quad (12) \end{aligned}$$

where

$$z_0 = \begin{cases} 1 & \text{if} \quad (Q_T/q) \geq 1 \\ Q_T/q & \text{if} \quad z < (Q_T/q) < 1 \\ z & \text{if} \quad (Q_T/q) \leq z. \end{cases}$$

Unlike Δ_S, the non-Sudakov form factor Δ_{NS} is not just a function of the branching variables, but depends on the history of the cascade via

$$Q_T = |\boldsymbol{q}_T + \boldsymbol{q}'_T + \boldsymbol{q}''_T + \ldots|. \quad (13)$$

Actually the recursion relation (9) is satisfied by a more inclusive distribution $F_n(x, Q_T, Q)$ in which the z, q dependence of $\mathcal{F}_n$ is integrated over, subject to the maximum angle specified by Q [13]. That is, if we introduce a distribution for n-gluon emission defined by

$$F_n(x, Q_T, Q) \equiv \int_x^1 dz \int \frac{d^2q}{\pi q^2} \Theta(Q - zq)\Delta_S(Q, zq)\mathcal{F}_n(x, Q_T, z, q), \quad (14)$$

then the recursion relation (9) becomes

$$F_n(x, Q_T, Q) = \int_x^1 \frac{dz}{z} \int \frac{d^2q}{\pi q^2} \Theta(Q - zq)\Delta_S(Q, zq)\tilde{P}(z, q, Q_T) F_{n-1}\left(\frac{x}{z}, Q'_T, q\right). \quad (15)$$

Finally we obtain the (scale-dependent unintegrated) gluon density by summing over all gluon emissions

$$F(x, Q_T, Q) = \sum_{n=0}^{\infty} F_n(x, Q_T, Q). \quad (16)$$

From (15) we find

$$\begin{aligned} F(x, Q_T, Q) &= F^0(x, Q_T, Q) + \\ &\quad + \int_x^1 dz \int \frac{d^2q}{\pi q^2} \Theta(Q - zq)\Delta_S(Q, zq)\tilde{P}(z, q, Q_T) F\left(\frac{x}{z}, Q'_T, q\right), \quad (17) \end{aligned}$$

with $Q'_T = |\boldsymbol{Q}_T + (1-z)\boldsymbol{q}|$. The inhomogeneous or "no-rung" contribution, F^0, may be regarded as the non-perturbative driving term. This basic integral equation (17), for the gluon structure function $F(x, Q_T, Q)$, which we have called the CCFM equation after its originators, is the starting point of our analysis. It may be approximated both at moderate x to yield the Altarelli-Parisi evolution equation, and at small x to yield the BFKL equation, as we shall now show.

3. Approximations in the small x region

To explore the structure of the gluon in the small x region we may approximate (17) by

$$F(x,Q_T,Q) = F^0(x,Q_T,Q) + \overline{\alpha}_S \int_x^1 \frac{dz}{z} \int \frac{d^2q}{\pi q^2} \Theta(Q-zq) \Delta_{NS}(z,q,Q_T) F\left(\frac{x}{z}, |\boldsymbol{Q}_T + \boldsymbol{q}|, q\right) \quad (18)$$

where we have set $\Delta_S = 1$ and retained only the $1/z$ term in the splitting function $\tilde{P}$. We have also approximated $(1-z)q$ by q in the argument Q'_T of F. In this small x limit, the variable q reduces to the transverse momentum q_T of the emitted gluon, see eq. (8). This is the CCFM integral equation [11, 12, 13] which we solve to find the x, Q_T and Q dependence of the gluon distribution. The procedure that we adopt and the results that we obtain are presented in Section 4.

Also in Section 4 we compare the results obtained from the CCFM equation with those obtained in the double leading logarithm (DLL) approximation in which (18) reduces to

$$F(x,Q_T,Q) = F^0(x,Q_T,Q) + \overline{\alpha}_S \int_x^1 \frac{dz}{z} \int \frac{d^2q}{\pi q^2} \Theta(Q-q) F\left(\frac{x}{z}, |\boldsymbol{Q}_T + \boldsymbol{q}|, q\right). \quad (19)$$

To be precise the DLL approximation is obtained by setting $\Delta_{NS} = 1$ and by replacing the angular ordering, $\Theta(Q - zq)$, by ordering in transverse momentum, $\Theta(Q - q)$. This procedure becomes equivalent to the conventional DLL approximation for $xg(x, Q^2)$ after we integrate over Q_T, as in (4). Here we have the advantage that we can also display the Q_T dependence of the gluon distribution.

Before we present our numerical results it is informative to gain insight into the structure of the CCFM equation, (18). We can simplify the discussion by rewriting (18) in terms of the moment function

$$F_\omega(Q_T, Q) = \int_0^1 dx\; x^{\omega-1} F(x, Q_T, Q). \quad (20)$$

We obtain

$$F_\omega(Q_T,Q) = F^0_\omega(Q_T,Q) + \overline{\alpha}_S \int \frac{d^2q}{\pi q^2} H_\omega(Q,Q_T,q) F_\omega(|\boldsymbol{Q}_T + \boldsymbol{q}|, q) \quad (21)$$

where

$$\begin{aligned} H_\omega(Q,Q_T,q) &= \int_0^1 dz\; z^{\omega-1} \Theta(Q-zq) \Delta_{NS}(z,q,Q_T) & (22)\\ &= \Theta(Q-q) \int_0^1 dz\, z^{\omega-1} \Delta_{NS}(z,q,Q_T) \\ &\quad + \Theta(q-Q) \int_0^{Q/q} dz\, z^{\omega-1} \Delta_{NS}(z,q,Q_T). & (23) \end{aligned}$$

The curtailment of the range of integration in the second term is seen to be a direct consequence of angular ordering.

(a) Unfolding the equation

It is useful to unfold the kernel of (21) so that the real emission and virtual corrections terms appear on equal footing, i.e. to the same order in α_S. On the one hand this will allow us to make correspondence with the BFKL equation, and on the other hand it will guide us to the correct structure of the driving term $F^0(x, Q_T, Q)$ to be used as input for the CCFM equation, (18). To unfold the kernel we first integrate (23) by parts

$$\begin{aligned} H_\omega(Q,Q_T,q) &= \frac{1}{\omega}\Big[\Theta(Q-q)+(Q/q)^\omega\,\Theta(q-Q)\Delta_{NS}(z=Q/q,q,Q_T)\Big] \\ &\quad -\frac{\overline{\alpha}_S}{\omega}\int_0^1 dz\; z^{\omega-1}\int\frac{dk^2}{k^2}\Theta(Q-zq)\Theta(k-zq)\Theta(Q_T^2-k^2)\Delta_{NS}(z,q,Q_T) \\ &= \frac{1}{\omega}\Big[\Theta(Q-q)+(Q/q)^\omega\,\Theta(q-Q)\Delta_{NS}\left(z=Q/q,q,Q_T\right)\Big] \\ &\quad -\frac{\overline{\alpha}_S}{\omega}\int\frac{dk^2}{k^2}\Theta(Q_T^2-k^2)H_\omega(\min\{Q,k\},q,Q_T) \end{aligned} \tag{24}$$

where the last term has been simplified using (23). We insert (24) in (21) and express the final term in terms of $F_\omega - F^0_\omega$. We obtain

$$\begin{aligned} F_\omega(Q_T,Q) &= F^0_\omega(Q_T,Q)+\frac{\overline{\alpha}_S}{\omega}\int\frac{dq^2}{q^2}\Theta(Q_T^2-q^2)F^0_\omega(Q_T,\min\{Q,q\}) \\ &+ \frac{\overline{\alpha}_S}{\omega}\int\frac{d^2q}{\pi q^2}\Big\{\Big[\Theta(Q-q)+(Q/q)^\omega\Theta(q-Q)\Delta_{NS}(z=Q/q,q,Q_T)\Big]F_\omega(|\boldsymbol{Q}_T+\boldsymbol{q}|,q) \\ &- \Theta(Q_T^2-q^2)F_\omega(Q_T,\min\{Q,q\})\Big\} \end{aligned} \tag{25}$$

It remains to unfold the non-Sudakov form factor Δ_{NS}. In the Appendix A, we show that (25) then becomes

$$\begin{aligned} F_\omega(Q_T,Q) &= \frac{1}{\omega}\hat{F}^0_\omega(Q_T,Q)+\frac{\overline{\alpha}_S}{\omega}\int\frac{d^2q}{\pi q^2}\left[\Theta(Q-q)+\left(\frac{Q}{q}\right)^\omega\Theta(q-Q)\right]F_\omega(|\boldsymbol{Q}_T+\boldsymbol{q}|,q) \\ &- \frac{\overline{\alpha}_S}{\omega}\int\frac{d^2q}{\pi q^2}\Theta(Q_T^2-q^2)F_\omega(Q_T,q) \\ &+ \frac{\overline{\alpha}_S}{\omega}\Theta(Q_T^2-Q^2)\int_{Q^2}^{Q_T^2}\frac{d^2q}{\pi q^2}q^2\frac{\partial F_\omega(Q_T,q)}{\partial q^2}\log\left(\frac{q^2}{Q_T^2}\right)\left[\left(\frac{Q}{q}\right)^\omega-1\right] \end{aligned} \tag{26}$$

where the driving term of the unfolded equation is related to that of the folded equation by

$$\begin{aligned} \frac{1}{\omega}\hat{F}^0_\omega(Q_T,Q) &= F^0_\omega(Q_T,Q)+\frac{\overline{\alpha}_S}{\omega}\int\frac{d^2q}{\pi q^2}\Theta(Q_T^2-q^2)F^0_\omega(Q_T,q) \\ &- \frac{\overline{\alpha}_S}{\omega}\Theta(Q_T^2-Q^2)\int_{Q^2}^{Q_T^2}\frac{d^2q}{\pi q^2}q^2\frac{\partial F^0_\omega(Q_T,q)}{\partial q^2}\log\left(\frac{q^2}{Q_T^2}\right)\left[\left(\frac{Q}{q}\right)^\omega-1\right] \end{aligned} \tag{27}$$

The second term on the right hand side of (26) corresponds to real gluon emission without any "non-Sudakov" damping, but with angular ordering included (cf. (23)). The following two terms are the unfolded virtual corrections, which, if resummed, would lead to the non-Sudakov form factor Δ_{NS}. The inhomogeneous term $\hat{F}^0_\omega$ in the unfolded equation, (26), should not contain any virtual corrections, but F^0_ω in the folded equation, (18), may.

To solve (27) for F^0_ω in terms of $\hat{F}^0_\omega$ it is simplest to use the following representation for the driving term of the unfolded equation (26)

$$\frac{1}{\omega}\hat{F}^0_\omega(Q_T,Q) = \int_0^1 dx\, x^{\omega-1}\int_x^1 \frac{dz}{z}\int \frac{d^2q}{\pi q^2}\Theta(Q-qz)\Phi^0\Big(\frac{x}{z},|\boldsymbol{q}+\boldsymbol{Q}_T|,q\Big). \tag{28}$$

Then the solution of (27) is

$$F^0_\omega(Q_T,Q) = \int_0^1 dx\, x^{\omega-1}\int_x^1 \frac{dz}{z}\int \frac{d^2q}{\pi q^2}\Theta(Q-qz)\Delta_{NS}(z,q,Q_T)\Phi^0\Big(\frac{x}{z},|\boldsymbol{q}+\boldsymbol{Q}_T|,q\Big). \tag{29}$$

The above representation, (28), mirrors relation (14) which, for $n=0$, expresses the driving term $\hat{F}^0$ in terms of the non-perturbative input $\mathcal{F}_{n=0}$. In section 4 we will use (29) to specify the driving term $F^0(x,Q_T,Q)$ of the (folded) CCFM equation (18) in terms of an assumed form for the non-perturbative input function Φ^0.

(b) The BFKL limit

We may take the leading $\log 1/x$ approximation of the unfolded equation, (26), for the moments of the gluon distribution. This corresponds to retaining the leading terms in the $\omega \to 0$ limit. That is we set $(Q/q)^\omega = 1$ in (26), which then reduces to

$$F_\omega(Q_T,Q) = \frac{1}{\omega}\hat{F}^{0L}_\omega(Q_T,Q) + \frac{\overline{\alpha}_S}{\omega}\int \frac{d^2q}{\pi q^2}\Big[F_\omega(|\boldsymbol{Q}_T+\boldsymbol{q}|,q) - F_\omega(Q_T,q)\Theta(Q_T^2-q^2)\Big] \tag{30}$$

where $\hat{F}^{0L}_\omega$ is the BFKL limit of $\hat{F}^0_\omega$ of (27). We see that the equation (30) generates a moment function F_ω which is independent of Q. If we transform back from moment (ω) space to x space, then we obtain the BFKL equation

$$\frac{\partial F(x,Q_T)}{\partial \log(1/x)} = \overline{\alpha}_S\int \frac{d^2q}{\pi q^2}\Big[F(x,|\boldsymbol{Q}_T+\boldsymbol{q}|) - \Theta(Q_T^2-q^2)F(x,Q_T)\Big], \tag{31}$$

where we have neglected the derivative of the inhomogeneous term with respect to $\log(1/x)$. The two terms in the integral on the right hand side correspond to real and virtual gluon emission respectively.

(c) Cancellation of the real and virtual singularities

We first expose the cancellation of the singularities in the BFKL limit [9]. To do this we rewrite (30) with the "unresolved" real emissions (i.e. emissions with $q^2 < \mu^2$) separated out

$$\begin{aligned} F_\omega(Q_T) = \frac{1}{\omega}\hat{F}^{0L}_\omega(Q_T) \;&+\; \frac{\overline{\alpha}_S}{\omega}\int \frac{d^2q}{\pi q^2}\Big[F_\omega(|\boldsymbol{Q}_T+\boldsymbol{q}|)\Theta(\mu^2-q^2) - F_\omega(Q_T)\Theta(Q_T^2-q^2)\Big] \\ &+\; \frac{\overline{\alpha}_S}{\omega}\int \frac{d^2q}{\pi q^2}F_\omega(|\boldsymbol{Q}_T+\boldsymbol{q}|)\Theta(q^2-\mu^2). \end{aligned} \tag{32}$$

The singularities as $\mu^2 \to 0$ occur in the second term on the right hand side. To explicitly show the cancellation between the real and virtual contributions, we approximate the "unresolved" real emission contribution using $F_\omega(|\boldsymbol{Q}_T + \boldsymbol{q}|) \simeq F_\omega(Q_T)$, which is valid at small q, and obtain

$$\begin{aligned}\overline{\alpha}_S \int \frac{d^2q}{\pi q^2}\Big[F_\omega(|\boldsymbol{Q}_T + \boldsymbol{q}|)\Theta(\mu^2 - q^2) - F_\omega(Q_T)\Theta(Q_T^2 - q^2)\Big] \\ &= -\overline{\alpha}_S F_\omega(Q_T)\int_{\mu^2}^{Q_T^2}\frac{dq^2}{q^2} + \mathcal{O}(\mu^2) \\ &\simeq -F_\omega(Q_T)\,\overline{\omega}(Q_T^2, \mu^2) \end{aligned} \tag{33}$$

where

$$\overline{\omega}(Q_T^2, \mu^2) \equiv \overline{\alpha}_S \log(Q_T^2/\mu^2). \tag{34}$$

The result (33) is the residual virtual contribution to $\omega F_\omega(Q_T)$ which remains after the cancellation of the real and virtual singularities.

If we substitute (33) into (32), we obtain

$$F_\omega(Q_T) = \frac{\hat{F}_\omega^{0L}(Q_T)}{\omega + \overline{\omega}} + \frac{\overline{\alpha}_S}{\omega + \overline{\omega}}\int \frac{d^2q}{\pi q^2}\Theta(q^2 - \mu^2)F_\omega(|\boldsymbol{Q}_T + \boldsymbol{q}|), \tag{35}$$

which, when we transform back to x space, becomes

$$F(x, Q_T) = \int_x^1 \frac{dz}{z} z^{\overline{\omega}} \hat{F}^{0L}\Big(\frac{x}{z}, Q_T\Big) + \overline{\alpha}_S \int_x^1 \frac{dz}{z} z^{\overline{\omega}} \int \frac{d^2q}{\pi q^2}\Theta(q^2 - \mu^2) F\Big(\frac{x}{z}, |\boldsymbol{Q}_T + \boldsymbol{q}|\Big). \tag{36}$$

Equation (36) clearly corresponds to the "folded" BFKL equation in which we have resummed all the "unresolved" real emissions and **all** the virtual corrections.

We recognise the Regge-like form $z^{\overline{\omega}}$ of the non-Sudakov form factor Δ_{NS}^L in the folded BFKL equation, which screens the $z \to 0$ singularities. We can also make the identification of the form factor using (11), which in this case becomes

$$\begin{aligned}\Delta_{NS}^L(z, Q_T, \mu^2) &= \exp\Big\{-\overline{\alpha}_S \int_z^1 \frac{dz'}{z'}\int \frac{dk^2}{k^2}\Theta(Q_T^2 - k^2)\Theta(k^2 - \mu^2)\Big\} \\ &= \exp\Big\{-\overline{\alpha}_S \log(1/z)\log(Q_T^2/\mu^2)\Big\} \\ &= z^{\overline{\omega}}, \end{aligned} \tag{37}$$

where $\overline{\omega}$ is given in (34). Note that the driving term $\hat{F}_\omega^{0L}/\omega$ of the unfolded BFKL equation (32) is free of $\mu^2 \to 0$ singularities, whereas the driving term of the folded version of equation (35) or (36) contains, through $\overline{\omega}$, these μ^2 singularities.

In the same way we can introduce a resolution μ^2 into the unfolded CCFM equation, (26), so that

$$
\begin{aligned}
F_\omega(Q_T,Q) &= \frac{1}{\omega}\hat{F}^0_\omega(Q_T,Q) + \\
&+\frac{\overline{\alpha}_S}{\omega}\int\frac{d^2q}{\pi q^2}\left[\Theta(Q-q)+\left(\frac{Q}{q}\right)^\omega\Theta(q-Q)\right]\Theta(q^2-\mu^2)F_\omega(|\boldsymbol{Q}_T+\boldsymbol{q}|,q) \\
&-\frac{\overline{\alpha}_S}{\omega}\int\frac{d^2q}{\pi q^2}\Theta(Q_T^2-q^2)\Theta(q^2-\mu^2)F_\omega(Q_T,q) \\
&+\frac{\overline{\alpha}_S}{\omega}\Theta(Q_T^2-Q^2)\int_{Q^2}^{Q_T^2}\frac{d^2q}{\pi q^2}q^2\frac{\partial F_\omega(Q_T,q)}{\partial q^2}\log\left(\frac{q^2}{Q_T^2}\right)\left[\left(\frac{Q}{q}\right)^\omega-1\right]. \qquad (38)
\end{aligned}
$$

After resumming all the virtual corrections and "unresolved" radiation we obtain, in analogy with (21)

$$
F_\omega(Q_T,Q)=\tilde{F}^0_\omega(Q_T,Q;\mu^2)+\overline{\alpha}_S\int\frac{d^2q}{\pi q^2}\tilde{H}_\omega(Q,Q_T,q;\mu^2)F_\omega(|\boldsymbol{Q}_T+\boldsymbol{q}|,q)\Theta(q^2-\mu^2) \qquad (39)
$$

with

$$
\tilde{H}_\omega(Q,Q_T,q;\mu^2)=\int dz\ z^{\omega-1}\Theta(Q-qz)\tilde{\Delta}_{NS}(z,q,Q_T;\mu^2) \qquad (40)
$$

where now the non-Sudakov form factor is of the form

$$
\tilde{\Delta}_{NS}(z,q,Q_T;\mu^2)=\exp\left(-\overline{\alpha}_S\int_z^1\frac{dz'}{z'}\int\frac{dk^2}{k^2}\Theta(Q_T^2-k^2)\Theta(k-z'q)\Theta(k^2-\mu^2)\right). \qquad (41)
$$

The driving term of (39) has a similar form to (29) except that the introduction of the resolution cut-off leads to a factor $\Theta(q^2-\mu^2)$ and to Δ_{NS} being replaced by $\tilde{\Delta}_{NS}$ of (41)

$$
\tilde{F}^0_\omega(Q_T,Q;\mu^2)=\int_0^1 dx\ x^{\omega-1}\int_x^1\frac{dz}{z}\int\frac{d^2q}{\pi q^2}\Theta(Q-qz)\Theta(q^2-\mu^2)\tilde{\Delta}_{NS}(z,q,Q_T;\mu^2)\Phi^0\Big(\frac{x}{z},|\boldsymbol{q}+\boldsymbol{Q}_T|,q\Big). \qquad (42)
$$

In fact we do not need to introduce a lower cut-off μ^2 on the dq^2 integration in (18), since the equation remains finite as $q\to 0$. However, here we have demonstrated the modifications necessary if, for pragmatic reasons, a cut-off is introduced. In particular we see Δ_{NS} of (11) must be replaced by $\tilde{\Delta}_{NS}$ of (41). The results will, of course, be independent of the choice of the resolution μ^2, up to $\mathcal{O}(\mu^2/Q_T^2)$.

Although the unfolded CCFM equation, (26), reduces to the BFKL equation in the leading $\log(1/x)$ (or leading $\overline{\alpha}_S/\omega$) approximation and although both equations are free from singularities at $q^2=0$, the details of the cancellations are different [15]. In the BFKL case the real emission terms and the virtual corrections are individually divergent and have to be separately regulated by the $q^2=\mu^2$ cut-off. On the other hand, for the CCFM equation both terms are **finite**, yet they generate additional powers of $1/\omega$. To be precise, when we solve eq. (26) iteratively we find after n iterations that

$$
F^{(n)}_\omega(Q_T,q)\sim\frac{1}{\omega^n}q^\omega\log^n(q/Q_T) \qquad (43)
$$

as $q \to 0$. The factor q^ω regulates the integrals at $q^2 = 0$ and keeps both the real and virtual terms finite, yet they separately contain double logarithmic factors, $(\log^2(1/x))^n$, arising from the behaviour of the integral

$$\frac{1}{\omega^n}\int_0 \frac{dq^2}{q^2} q^\omega \log^n\left(\frac{q^2}{Q_T^2}\right) \sim \frac{1}{\omega^{2n+1}}. \tag{44}$$

The $(\log(1/x))^{2n}$ behaviour exactly cancels between the real emission and the virtual correction terms.

4. Numerical solution of the CCFM equation

We explore the structure of the gluon distribution $F(x, Q_T, Q)$ at small x by numerically solving the CCFM equation (18). To be precise we solve the equation in the presence of the μ^2 resolution cut-off (cf. (39))

$$F(x,Q_T,Q) = F^0(x,Q_T,Q;\mu^2) + \int_x^1 \frac{dz}{z}\int \frac{d^2q}{q^2}\overline{\alpha}_S \Theta(Q - zq)\Theta(q^2-\mu^2)\tilde{\Delta}_{NS}(z,q,Q_T;\mu^2)F(\frac{x}{z},Q_T',q) \tag{45}$$

with $Q_T' = |\boldsymbol{Q}_T + (1-z)\boldsymbol{q}|$, and where the non-Sudakov form factor $\tilde{\Delta}_{NS}$ is evaluated using (41). We take the argument of α_S to be Q_T^2 since this value is usually assumed for small x studies involving the BFKL equation.

From (42) we see that the driving term is given by

$$F^0(x,Q_T,Q;\mu^2) = \int_x^1 \frac{dz}{z}\int \frac{d^2q}{\pi q^2}\Theta(Q-qz)\Theta(q^2-\mu^2)\tilde{\Delta}_{NS}(z,q,Q_T;\mu^2)\Phi^0\Big(\frac{x}{z},|\boldsymbol{q}+\boldsymbol{Q}_T|,q\Big). \tag{46}$$

In general Φ^0 will contain some smearing in q. However, this is an inessential complication and it is sufficient to assume strong-ordering in transverse momenta and to take the q dependence of Φ^0 to be $\delta(\boldsymbol{q}+\boldsymbol{Q}_T)$. The x/z and Q_T dependence of Φ^0 are chosen so that if the Θ functions and $\tilde{\Delta}_{NS}$ were to be set equal to 1 in (46), then F^0 would reduce to $3(1-x)^5 N\exp(-Q_T^2/Q_0^2)$. The normalisation N is fixed so that the gluon, integrated over all Q_T^2, carries half the momentum of the proton. Q_0^2 is taken to be 1 GeV^2. These assumptions are equivalent to the choice

$$\begin{aligned} F^0(x,Q_T,Q;\mu^2) &= N\exp(-Q_T^2/Q_0^2)\int_x^1 \frac{dz}{z}\Theta(Q-Q_Tz)\Theta(Q_T^2-\mu^2) \\ &\quad \tilde{\Delta}_{NS}(z,Q_T,Q_T;\mu^2)\frac{d[3(1-x/z)^5]}{d\log(z/x)}. \end{aligned} \tag{47}$$

We solve (45) by iteration starting from the input form given in (47). We restrict the iterative procedure to the domain[4] $Q_T^2, Q_T'^2 > Q_0^2 = 1$ GeV^2. We take the upper limit cut-off,

[4]Strictly speaking the non-Sudakov form factor, (41), is also dependent on Q_0^2 to ensure complete cancellation of the real and virtual emissions.

Q_F^2, on the q^2 integrations to be in the region $10^4 - 10^5\,\mathrm{GeV}^2$, though the results are insensitive to variations around and above these values. We use a lower cut-off μ^2, although we saw in Section 3 that the CCFM equation is well behaved in the $\mu^2 \to 0$ limit.

Clearly, therefore, the results should be independent of the choice of the resolution μ^2, up to contributions of $\mathcal{O}(\mu^2/Q_T^2)$ and $\mathcal{O}(\mu^2/Q^2)$. This is well demonstrated by the sample of results shown in Figs. 4 and 5 which correspond to the choices $\mu^2 = 10^{-2}, 10^{-1}, 0.5$ and, $1\,\mathrm{GeV}^2$. The convergence to a stable result with decreasing μ^2 is a test of the consistency of the solution. From now on we show results for the choice $\mu^2 = 10^{-2}\,\mathrm{GeV}^2$.

(a) CCFM solutions compared with those of the DLL approximation

Starting from the input of (47) we iterate (45) until a stable result for $F(x, Q_T, Q)$ is obtained. The numerical procedure is outlined in appendix B. We take $Q_F^2 = 10^5\,\mathrm{GeV}^2$. The whole calculation is repeated using the double-leading-logarithm (DLL) approximation in which we replace angular ordering, $\Theta(Q - zq)$, by ordering in transverse momenta, $\Theta(Q - q)$, and in which we set $\Delta_{NS} = 1$.

Figs. 6, 7 and 8 respectively show a representative sample of results for the Q, Q_T and x dependence of the gluon distribution in the small x regime. The three plots of Fig. 6 compare the Q^2 dependence of $F(x, Q_T, Q)$ obtained from the CCFM and DLL equations, for $Q_T^2 = 1, 10$ and $100\,\mathrm{GeV}^2$ respectively. We see that F obtained from the CCFM equation is less dependent on Q^2 than the DLL values of F. In the DLL case the suppression of F in the region $Q^2 \lesssim Q_T^2$ is simply a reflection of the ordering of transverse momenta that is embodied in the equation; an ordering which is not, in fact, appropriate in the small x domain. Recall that in the BFKL leading $\log(1/x)$ limit F becomes independent of Q^2. The CCFM solutions in Fig. 6 exhibit this behaviour for the larger values of Q^2, but for smaller Q^2 they show that non-leading $\log(1/x)$ contributions begin to become important. The low Q^2 region is where the physically motivated angular ordering embodied in the CCFM equation (but not in the BFKL equation) provides more of a constraint.

Fig. 7 shows the Q_T distributions of the gluon obtained from solving the CCFM equation and from the approximate DLL equation. As before the DLL solutions satisfy $Q_T^2 \lesssim Q^2$ even at the smallest values of x, which again reflect the transverse momentum ordering, $\Theta(Q-q)$, contained in equation (19). On the other hand the CCFM solutions become significantly broader in Q_T, with decreasing x, on account of the more appropriate angular ordering constraint $\Theta(Q - zq)$. The extensive Q_T tail is a key property which characterises the gluon distribution in the small x domain.

Fig. 8 shows the behaviour of the integrated gluon distribution, $xg(x, Q^2)$ of (4) with lower limit Q_0^2, as a function of x for various values of Q^2. Note that the gluon distributions are generated radiatively from an input which is "flat" at small x, (46), and so the rapid rise of xg with decreasing x (shown as continuous curves) is generated by the CCFM equation. To quantify the increase, we show in Fig. 9 the effective value of λ, defined by

$$xg(x, Q^2) = Ax^{-\lambda}. \tag{48}$$

For small x we see that the solutions converge to a typical $x^{-0.5}$ behaviour, approximately independent of Q^2, which, as we shall see below, is consistent with that obtained from the solution of the (leading $\log(1/x)$) BFKL equation.

The dashed curves in Figs. 8 and 9 show the characteristic double-leading-logarithm (DLL) small x behaviour

$$xg(x,Q^2) \sim \exp\Big[2\{\xi(Q^2,Q_0^2)\log(1/x)\}^{\frac{1}{2}}\Big] \tag{49}$$

appropriate to a "flat" input, that is $xg(x,Q_0^2) \to$ constant as $x \to 0$. In (49) we have omitted slowly varying functions of the argument of the exponential. We see that the steepness or "effective slope" λ increases with Q^2 via the "evolution length"

$$\xi(Q^2,Q_0^2) = \int_{Q_0^2}^{Q^2} \frac{dq^2}{q^2}\overline{\alpha}_S(q^2). \tag{50}$$

This behaviour is clearly evident in the DLL results of Figs. 8 and 9. The difference with the CCFM predictions for small $x, x \lesssim 10^{-2}$, shows the importance of implementing angular ordering in this domain.

(b) Comparison with solutions of the BFKL equation

To investigate the small x limit we compare the CCFM solutions with those that we obtained by solving the BFKL equation with the same driving term. To be precise we solve the unfolded BFKL equation

$$\begin{aligned} F(x,Q_T) &= F^{0L}(x,Q_T) + \\ &+ \overline{\alpha}_S(Q_T^2)\int_x^1 \frac{dz}{z}\int_{Q_0^2}^{\infty}\frac{dQ_T'^2}{Q_T'^2}\left\{\frac{Q_T'^2F(z,Q_T') - Q_T^2F(z,Q_T)}{|Q_T'^2 - Q_T^2|} + \frac{Q_T^2F(z,Q_T)}{(4Q_T'^4+Q_T^4)^{\frac{1}{2}}}\right\} \end{aligned} \tag{51}$$

with the driving term

$$F^{0L}(x,Q_T) = 3(1-x)^5N\exp(-Q_T^2/Q_0^2). \tag{52}$$

The integration region is restricted to $Q_T'^2 > Q_0^2 = 1$ GeV^2. For completeness, we show in Appendix C that, for fixed coupling α_S and $Q_0^2 = 0$, the BFKL equation (51) can be rewritten in the form

$$F(x,Q_T) = F^{0L}(x,Q_T) + \overline{\alpha}_S\int_x^1\frac{dz}{z}\int\frac{d^2q}{\pi q^2}\Big[F(x,|\boldsymbol{Q}_T+\boldsymbol{q}|) - \Theta(Q_T^2-q^2)F(x,Q_T)\Big], \tag{53}$$

which we obtained previously, see (31).

Fig. 10 compares the properties of the integrated gluons obtained from solving the CCFM and BFKL equations, while Fig. 9 shows the resulting effective slopes λ. Since the solution, $F(x,Q_T)$, of the BFKL equation is independent of Q, the Q^2 dependence observed for xg comes entirely from the Q_T integration of (4). On the other hand the solution $F(x,Q_T,Q)$ of the CCFM equation has an intrinsic Q dependence arising from angular-ordering, $\Theta(Q-qz)$. As a consequence we see from Fig. 10 that the CCFM gluon evolves faster with Q^2. From Fig.

9 we note that the effective slopes λ of the integrated CCFM and BFKL gluons are remarkably similar at small x. We conclude that the next-to-leading $\log(1/x)$ effects included in the CCFM formalism have a comparatively weak effect on the $x^{-\lambda}$ behaviour, although we note that the onset of the $x^{-\lambda}$ form is more delayed for the CCFM solution.

5. Conclusions

We have solved a unified equation for the unintegrated gluon distribution which incorporates BFKL dynamics at small x and Altarelli-Parisi evolution at larger x. We called it the CCFM equation after its originators — Catani, Ciafaloni, Fiorani and Marchesini. Starting from a driving term based on a "flat" $3(1-x)^5$ gluon with a narrow Q_T distribution, $\exp(-Q_T^2/Q_0^2)$, we used an iterative procedure to find the x, Q_T and Q dependence of the gluon.

We concentrated on the behaviour of the gluon in the small x regime. The key ingredients of the CCFM equation are the angular-ordering of gluon emissions and the presence of a non-Sudakov form factor. We found that the CCFM equation generates a gluon $F(x, Q_T, Q)$ with a singular $x^{-\lambda}$ behaviour, with $\lambda \simeq 0.5$, and a Q_T distribution which broadens and develops a significant tail as x decreases. Moreover the angular-ordering introduces a dependence of the unintegrated gluon on the scale Q, especially at the lower values of Q^2. Sample results are shown in Figs. 6–9. It is convenient to display the x dependence of the integrated distribution, xg of (4), although we should recall that the physically relevant quantity at small x is the unintegrated distribution $F(x, Q_T, Q)$.

We compared the CCFM solutions with the conventional DLL approximation in which angular-ordering is replaced by strong-ordering in the gluon transverse momenta and in which the non-Sudakov form factor is omitted, $\Delta_{NS} = 1$. The gluon is then found to be much less steep with decreasing x and to have a narrower Q_T distribution. We found that the DLL approximation starts to differ from the CCFM results in the region $x \lesssim 10^{-2}$.

We then compared the CCFM solutions with the solutions of the BFKL approximation, based on an equation in which the angular-ordering is ignored, and which therefore has unintegrated solutions $F(x, Q_T)$ which do not depend on the scale Q. In fact the gluon $g(x, Q^2)$ obtained from the BFKL equation acquires its Q^2 dependence entirely from the integration in (4). As a consequence we find that the integrated BFKL solutions evolve more slowly in Q^2 than those obtained from the CCFM equation, which have an additional intrinsic Q^2 dependence as shown, for example, in Fig. 6. Fig. 9 quantifies the $x^{-\lambda}$ agreement between the unified CCFM solution and the approximate BFKL solution. The agreement is remarkably good at small x, especially at the larger values of Q^2. Both the CCFM and BFKL solutions have a behaviour $xg \sim x^{-\lambda}$ at small x, where the value of λ is in the region of 0.5 with only a modest dependence on Q^2, in contrast to the dependence of λ on the evolution length for the DLL approximation, see Fig. 9.

It is appropriate to add a word of caution. Our study has concentrated on obtaining the perturbative QCD predictions of the behaviour of the gluon at small x. In particular we have

made the small x approximation for the splitting function (7)

$$\tilde{P} \simeq \overline{\alpha}_S \Delta_{NS} \frac{1}{z} \tag{54}$$

and we have set the Sudakov form factor $\Delta_S = 1$.

In other words we have neglected the singularity at $z = 1$ and its Sudakov suppression. Moreover we have neglected the effect of the flavour singlet quarks on the evolution of the gluon. Although these may be viewed as moderate-to-large x effects, they may, to some extent, feed through to small x leading to possible next-to-leading $\log(1/x)$ contributions to $F(x, Q_T, Q)$. Therefore, at this stage, our results should be regarded as illustrative of the main properties of the gluon distribution at small x, and as an indication of the respective domains of validity of BFKL and conventional Altarelli-Parisi dynamics. To obtain a quantitative prediction of the gluon for all x we must include a proper treatment of the $z = 1$ behaviour and include the quark distributions .

Acknowledgements

We thank G. Marchesini and B. R. Webber for valuable discussions. J. K. thanks the Department of Physics and Grey College of the University of Durham for their warm hospitality. This work has been supported in part by the UK Particle Physics and Astronomy Research Council, the Polish KBN-British Council collaborative research programme, the KBN grant no. 2 P302 062 04 and the EU under contracts no. CHRX-CT92-0004/CT93-0357.

Appendix A : Unfolding the CCFM equation

Here we derive the "unfolded" version of the CCFM equation, which is shown in (26). We start by unfolding the non-Sudakov form factor Δ_{NS} in (25). The relevant term is

$$\begin{aligned} &\int_{Q^2}^{\infty} \frac{d^2q}{\pi q^2} \left(\frac{Q}{q}\right)^{\omega} \Delta_{NS}(z = Q/q, q, Q_T) F_\omega(|\boldsymbol{Q}_T + \boldsymbol{q}|, q) \\ &\qquad = Q^\omega G_\omega(Q, Q_T) \; + \; \int_{Q^2}^{\infty} \frac{d^2q}{\pi q^2} \Big(\frac{Q}{q}\Big)^{\omega} F_\omega(|\boldsymbol{Q}_T + \boldsymbol{q}|, q) \end{aligned} \tag{55}$$

with

$$G_\omega(Q, Q_T) \equiv \int_{Q^2}^{\infty} \frac{d^2q}{\pi q^2} \Big(\frac{1}{q^\omega}\Big) [\Delta_{NS}(z = Q/q, q, Q_T) - 1] F_\omega(|\boldsymbol{Q}_T + \boldsymbol{q}|, q), \tag{56}$$

where we have simply subtracted and added 1 to Δ_{NS}. For $Q_T^2 < Q^2$ the unfolding is trivial since, then $\Delta_{NS}(z = Q/q, q, Q_T) = 1$, see (12). This leaves the case $Q_T^2 > Q^2$. From the form of Δ_{NS} we see that $G_\omega(Q_T, Q_T) = 0$, and so we may write

$$G_\omega(Q, Q_T) = \int_{Q^2}^{Q_T^2} \frac{dQ'^2}{Q'^2} \left[- \frac{\partial G_\omega(Q', Q_T)}{\partial \log Q'^2} \right]. \tag{57}$$

If we differentiate (56) we obtain

$$
\begin{aligned}
-\frac{\partial G_\omega(Q',Q_T)}{\partial \log Q'^2} &= -\int_{Q'^2}^{\infty}\frac{d^2q}{\pi q^2}\frac{1}{q^\omega}\frac{\partial \Delta_{NS}(z=Q'/q,q,Q_T)}{\partial \log Q'^2}F_\omega(|\boldsymbol{Q}_T+\boldsymbol{q}|,q)\\
&= \frac{1}{Q'^\omega}\int_{Q'^2}^{\infty}\frac{d^2q}{\pi q^2}\Big(\frac{Q'}{q}\Big)^\omega\,\frac{\overline{\alpha}_S}{2}\log\Big(\frac{Q'^2}{Q_T^2}\Big)\Delta_{NS}\Big(z=\frac{Q'}{q},q,Q_T\Big)F_\omega(|\boldsymbol{Q}_T+\boldsymbol{q}|,q)\\
&= \frac{1}{Q'^\omega}\log\Big(\frac{Q'^2}{Q_T^2}\Big)\left[\frac{\partial F_\omega(Q_T,Q')}{\partial \log Q'^2}-\frac{\partial F^0_\omega(Q_T,Q')}{\partial \log Q'^2}\right] \qquad (58)
\end{aligned}
$$

where the last equality is evident once we differentiate (21). Successively inserting (58) into (57), (55) and (25) we obtain the $(Q/q)^\omega$ contribution to the last term in square brackets in (26) and (27).

It remains to evaluate the term containing $F_\omega(Q_T,\min\{Q,q\})$ in (25). We may rewrite this term as

$$
-\frac{\overline{\alpha}_S}{\omega}\int\frac{d^2q}{\pi q^2}\Theta(Q_T^2-q^2)\Big\{F_\omega(Q_T,q)\Big[1-\Theta(q-Q)\Big]+F_\omega(Q_T,Q)\Theta(q-Q)\Big\}. \qquad (59)
$$

We immediately identify the term with 1 in the square brackets as one of the terms in (26). We are left with two contributions from (59), each containing $\Theta(q-Q)$, which combine to become

$$
\frac{\overline{\alpha}_S}{\omega}\int_{Q^2}^{Q_T^2}\frac{d^2q}{\pi q^2}\Big\{F_\omega(Q_T,q)-F_\omega(Q_T,Q)\Big\}=-\frac{\overline{\alpha}_S}{\omega}\int_{Q^2}^{Q_T^2}\frac{d^2q}{\pi q^2}\frac{\partial F_\omega(Q_T,q)}{\partial\log q^2}\log\Big(\frac{q^2}{Q_T^2}\Big), \qquad (60)
$$

where the last equality follows on integrating by parts. We have now deduced (26), and (27), from (25).

Appendix B : Numerical technique used to solve CCFM equation

We briefly describe the numerical technique that we used to solve the integral equation, (45), for the gluon distribution $F(x,Q_T,Q)$. The starting point is the (double) expansion of the function $f(x,Q_T,Q)=Q_T^2F(x,Q_T,Q)$ in terms of the Tchebyshev polynomials with their arguments being linear functions of the variables $\log(Q_T^2/\Lambda^2)$ and $\log(Q^2/\Lambda^2)$. To be precise we map the regions $Q_0^2<Q_T^2<Q_F^2$ and $\mu^2<Q^2<Q_F^2$ into the interval (–1, 1) introducing respectively the variables

$$
\begin{aligned}
\tau_T &= 2\log\left(\frac{Q_T^2}{Q_FQ_0}\right)/\log\left(\frac{Q_F^2}{Q_0^2}\right)\\
\tau &= 2\log\left(\frac{Q^2}{Q_F\mu}\right)/\log\left(\frac{Q_F^2}{\mu^2}\right). \qquad (61)
\end{aligned}
$$

We then expand the function f in the polynomial form

$$
f(x,Q_T,Q)=\sum_{i,j=1}^{N}C_i(\tau_T)C_j(\tau)f_{ij}(x) \qquad (62)
$$

where the functions $f_{ij}(x)$ are the values of $f(x, Q_T, Q)$ at the "nodes" Q_{Ti}^2 and Q_j^2 specified by

$$\frac{Q_{Ti}^2}{Q_F Q_0} = \left(\frac{Q_F}{Q_0}\right)^{\tau_i}, \qquad \frac{Q_j^2}{Q_F \mu} = \left(\frac{Q_F}{\mu}\right)^{\tau_j}, \tag{63}$$

with τ_k defined by

$$\tau_k = \cos\{(k - \tfrac{1}{2})\pi/N\}. \tag{64}$$

The functions $C_k(\tau)$ in (62) are obtained from the Tchebyshev polynomials $T_n(\tau)$ as follows

$$C_k(\tau) = \frac{1}{2N} \sum_{n=1}^{N} v_n T_n(\tau) T_n(\tau_k) \tag{65}$$

where $v_1 = \frac{1}{2}$ and $v_n = 1$ for $n > 1$. In this way we can achieve a good approximation to the Q_T and Q dependence of f in terms of a modest number N of Tchebyshev polynomials. Typically we take $N = 10$.

We now substitute the expansion (62) into the CCFM equation (45) and obtain the following set of Volterra-type integral equations for $f_{ij}(x)$

$$f_{ij}(x) = f_{ij}^0(x) + \int_x^1 \frac{dz}{z} \sum_{k,\ell=1}^{N} A_{ij,k\ell}(z) f_{k\ell}(x/z) \tag{66}$$

where the driving term

$$f_{ij}^0(x) = Q_{Ti}^2 F^0(x, Q_{Ti}, Q_j), \tag{67}$$

and the kernel

$$\begin{aligned} A_{ij,k\ell}(z) &= Q_{Ti}^2 \, \overline{\alpha}_S(Q_{Ti}^2) \int_0^\pi d\phi \int \frac{dq^2}{\pi q^2 Q_{Ti}'^2} \Theta(Q_j - qz) \Theta(Q_F^2 - q^2) \Theta(q^2 - \mu^2) \\ &\quad \Theta(Q_{Ti}'^2 - Q_0^2) \tilde{\Delta}_{NS}(z, q, Q_{Ti}, \mu^2) C_k(\tau) \; C_\ell(\tau). \end{aligned} \tag{68}$$

Here we have

$$Q_{Ti}'^2 = |\boldsymbol{Q}_T + \boldsymbol{q}(1-z)|^2 = Q_{Ti}^2 + (1-z)^2 q^2 + 2(1-z) q Q_{Ti} \cos\phi \tag{69}$$

and the non-Sudakov form factor $\tilde{\Delta}_{NS}$ of (41). The set of equations of (66) is solved for the $f_{ij}(x)$ by iteration and the function $f(x, Q_T, Q)$ then determined from (62).

Appendix C : Different forms of the BFKL equation

Here we show the equivalence of the forms of the BFKL equation given in (51) and (53). We start from (51) and write it in the form of a two-dimensional integration over d^2Q_T'. It

is convenient to introduce a regulator δ^2 and to combine the two virtual contributions which contain $F(z,Q_T)$. Then (51), with $Q_0^2=0$, gives

$$\begin{aligned} F(x,Q_T) &= F^{0L}(x,Q_T)+ \\ &+ \lim_{\delta^2\to 0}\overline{\alpha}_S\int_x^1\frac{dz}{z}\int\frac{d^2Q'_T}{\pi}\frac{1}{|\boldsymbol{Q}'_T-\boldsymbol{Q}_T|^2+\delta^2}\left\{F(z,Q'_T)-\frac{Q_T^2F(z,Q_T)}{[Q_T'^2+|\boldsymbol{Q}'_T-\boldsymbol{Q}_T|^2+\delta^2]}\right\}. \end{aligned} \tag{70}$$

We introduce an integration over the Feynman parameter λ to express the virtual contribution in (70) in the form

$$\begin{aligned} I &\equiv Q_T^2\int\frac{d^2Q'_T}{\pi}\frac{1}{[|\boldsymbol{Q}'_T-\boldsymbol{Q}_T|^2+\delta^2][Q_T'^2+|\boldsymbol{Q}'_T-\boldsymbol{Q}_T|^2+\delta^2]} \\ &= Q_T^2\int_o^1 d\lambda\int\frac{d^2Q'_T}{\pi}\frac{1}{[\lambda Q_T'^2+|\boldsymbol{Q}'_T-\boldsymbol{Q}_T|^2+\delta^2]^2}. \end{aligned} \tag{71}$$

If we now make the substitution

$$Q'_T\to Q'_T+\frac{Q_T}{\lambda+1}$$

then we can easily perform the $d^2Q'_T$ and $d\lambda$ integrations and obtain

$$\begin{aligned} I &= \log\left(\frac{Q_T^2}{\delta^2}\right)+\mathcal{O}(\delta^2/Q_T^2) \\ &= \int_{\delta^2}^{Q_T^2}\frac{d^2q}{\pi q^2}+\mathcal{O}(\delta^2/Q_T^2). \end{aligned} \tag{72}$$

We now substitute the virtual contribution I of (72) back into (70) and change the variable of integration over the real emission contribution to $\boldsymbol{q}=\boldsymbol{Q}'_T-\boldsymbol{Q}_T$. In this way we obtain the form of the BFKL equation shown in (53).

References

[1] L.V. Gribov, E.M. Levin and M.G. Ryskin, Phys. Rep. **100** (1983) 1.

[2] For recent reviews of small x physics see e.g.: A.D. Martin, Acta. Phys. Polon. **B25** (1994) 265; A.D. Martin, Proc. Int. Conf. on HE Physics, July 1994, Glasgow; J. Kwiecinski, Proc. of the Workshop QCD94, July 1994, Montpellier, France; E. Laenen and E.M. Levin, Fermilab-Pub-93-350-T; S. Catani, invited talk at Les Rencontres de Physique de la Valee d'Aosta, "Results and Perspectives in Particle Physics", La Thuile, March 1994, Florence preprint DFF 207/6/94.

[3] J. Feltesse, Proc. Int. Conf. on HE Physics, July 1994, eds. P. J. Bussey and I. G. Knowles, Glasgow.

[4] See for example, J. C. Collins, D. E. Soper and G. Sterman in "Perturbative QCD", ed. A. H. Mueller, (World Scientific, Singapore, 1989), p. 1, and refs. therein.

[5] G. Altarelli and G. Parisi, Nucl. Phys. **B126** (1977) 298; E. Reya, Phys. Rep. **69** (1981) 195; G. Altarelli, Phys. Rep. **81** (1982) 1.

[6] Yu. L. Dokshitzer, Sov. Phys. JETP **46** (1977) 641.

[7] S. Catani, M. Ciafaloni and F. Hautmann, Phys. Lett. **B242** (1990) 97; Nucl. Phys. **B366** (1991) 657; J. C. Collins and R. K. Ellis, Nucl. Phys. **B360** (1991) 3; S. Catani and F. Hautmann, Nucl. Phys. **B427** (1994) 475.

[8] E. A. Kuraev, L.N. Lipatov and V. Fadin, Zh. Eksp. Teor. Fiz. **72** (1977) 373 [Sov. Phys. JETP **45** (1977) 199]; Ya. Ya. Balitskij and L.N. Lipatov, Yad. Fiz. **28** (1978) 1597 [Sov. J. Nucl. Phys. **28** (1978) 822]; L.N. Lipatov, in "Perturbative QCD", ed. A.H. Mueller, (World Scientific, Singapore, 1989), p.411; J.B. Bronzan and R.L. Sugar, Phys. Rev. **D17** (1978) 585.

[9] T. Jaroszewicz, Acta. Phys. Polon. **B11** (1980) 965.

[10] A. J. Askew, J. Kwieciński, A. D. Martin and P. J. Sutton, Phys. Rev. **D49** (1994) 4402; A. J. Askew et al., Phys. Lett. **B325** (1994) 212.

[11] M. Ciafaloni, Nucl. Phys. **296** (1988) 49.

[12] S. Catani, F. Fiorani and G. Marchesini, Phys. Lett. **B234** (1990) 339; Nucl. Phys. **B336** (1990) 18.

[13] G. Marchesini, Proceedings of the Workshop "QCD at 200 TeV", Erice, Italy, June 1990, edited by L. Cifarelli and Yu.L. Dokshitzer, Plenum Press, New York, 1992, p. 183.

[14] G. Marchesini, Proceedings of the QCD94 Workshop, July 1994, Montpellier, France.

[15] G. Marchesini, Univ. of Milan preprint, IFUM-486-FT (November 1994).

[16] B.R. Webber, Nucl. Phys. B (Proceedings Supplement) **18C** (1990) 38.

[17] G. Marchesini and B.R. Webber, Nucl. Phys. **B386** (1992) 215; B.R. Webber, Proceedings of the Workshop "Physics at HERA", DESY, Hamburg, Germany, October 1992, edited by W. Buchmüller and G. Ingelman.

Figure Captions

Fig. 1 Gluon emission with probability given by (5).

Fig. 2 Multigluon emission in deep inelastic scattering of a proton.

Fig. 3 Kinematic variables for multigluon emission. The distribution $\mathcal{F}_n$ describing n gluon emission is given in terms of the distribution $\mathcal{F}_{n-1}$ for $n-1$ gluon emission in (9).

Fig. 4 The integrated gluon $xg(x,Q^2)$ calculated using (4) from the solution $F(x,Q_T,Q)$ of the CCFM equation (45) for different choices of the lower cut-off $q^2=\mu^2$ at each of five values of Q^2. Here we take $Q_F^2 = 10^4\,\mathrm{GeV}^2$. Recall that our solutions are obtained from a "flat" gluon input.

Fig. 5 The Q^2 dependence of the gluon distribution obtained by solving the CCFM equation (45) for different choices of the lower cut-off $q^2=\mu^2$ at each of two values of Q^2 and four values of small x. The values of μ^2 are as in Fig. 4. Here we take $Q_F^2 = 10^4\,\mathrm{GeV}^2$.

Fig. 6 The Q^2 dependence of the gluon distribution $F(x,Q_T,Q)$, obtained by solving the CCFM equation (45) (continuous curves), compared with that from the DLL equation (dashed curves), for (a) $Q_T^2 = 10$ GeV^2 and (b) $Q_T = 100$ GeV^2. In each case we show the Q^2 dependence for $x = 10^{-5}, 10^{-4}, 10^{-3}$ and 10^{-2}.

Fig. 7 The Q_T^2 dependence of the gluon distribution $F(x,Q_T,Q)$, obtained by solving the CCFM equation (45) (continuous curves) and the DLL equation (dashed curves), for (a) $Q^2 = 10$ GeV^2, (b) $Q^2 = 10^2$ GeV^2 and (c) $Q^2 = 10^3$ GeV^2. In each case we show curves for $x = 10^{-5}, 10^{-4}, 10^{-3}, 10^{-2}$ and 10^{-1}.

Fig. 8 The integrated gluon distribution xg versus x, obtained from both the CCFM (continuous curves) and the DLL (dashed curves) integral equations, for $Q^2 = 4, 10, 10^2, 10^3$ and 10^4 GeV^2. Recall that our solutions are obtained from a "flat" gluon input.

Fig. 9 The effective values of λ, defined by $xg = Ax^{-\lambda}$, obtained from the gluon distributions shown in Figs. 8 and 10. The CCFM values (continuous curves) are compared with those obtained from the BFKL (dot-dashed curves) and DLL approximations (dashed curves). In each case we show curves corresponding to the five different values of Q^2

Fig. 10 The integrated gluon distribution xg versus x, obtained from the CCFM (continuous curves) and the BFKL (dashed curves) equations for $Q^2 = 4, 10, 10^2, 10^3$ and $10^4\,\mathrm{GeV}^2$. Recall that our solutions are obtained from a "flat" gluon input.

This figure "fig1-1.png" is available in "png" format from:

http://arXiv.org/ps/hep-ph/9503266v1

This figure "fig1-2.png" is available in "png" format from:

http://arXiv.org/ps/hep-ph/9503266v1

This figure "fig1-3.png" is available in "png" format from:

http://arXiv.org/ps/hep-ph/9503266v1

This figure "fig1-4.png" is available in "png" format from:

http://arXiv.org/ps/hep-ph/9503266v1

Fig. 4

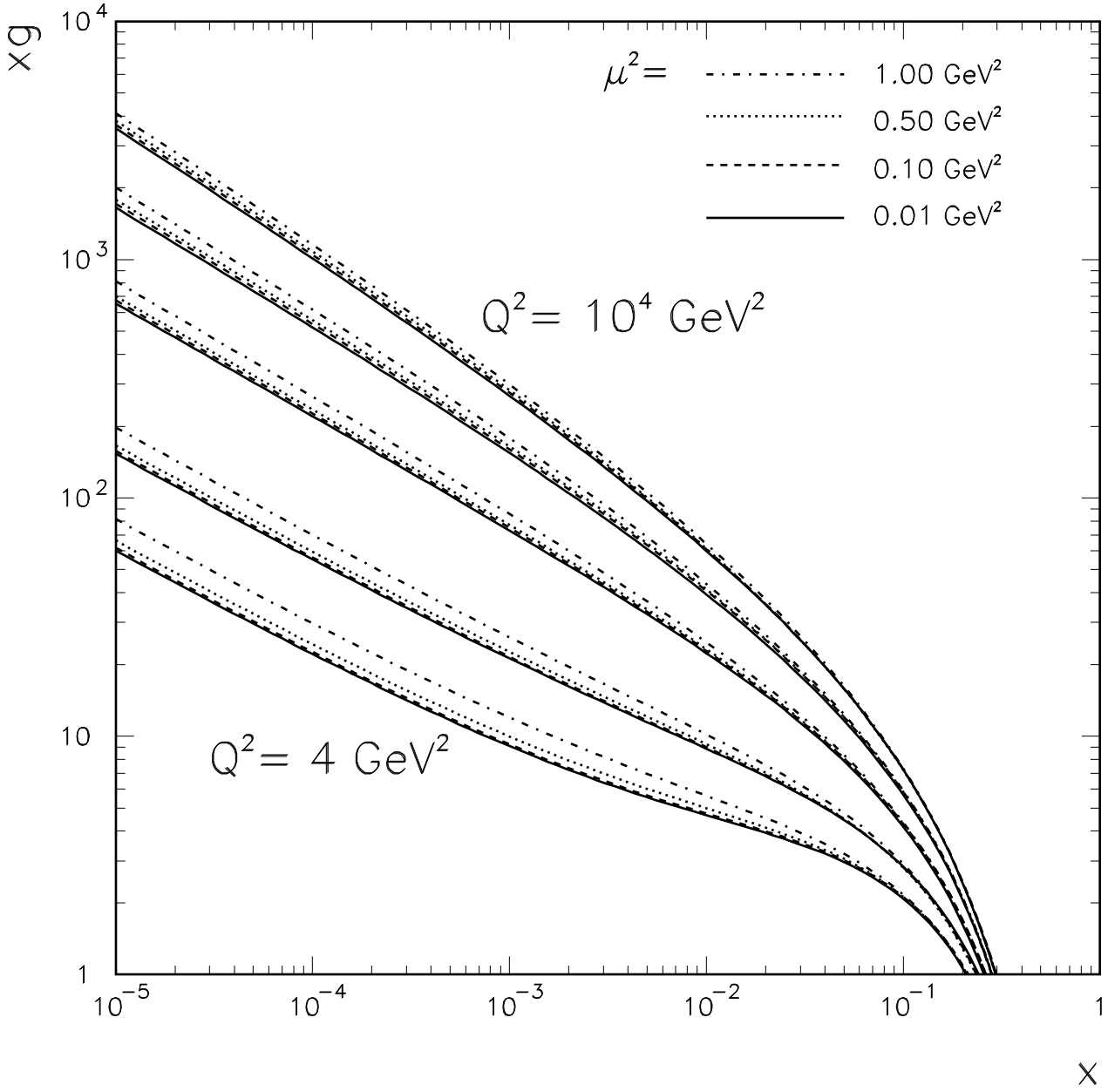
xg
X
$\mu^2=$
1.00 GeV²
0.50 GeV²
0.10 GeV²
0.01 GeV²
$Q^2= 10^4$ GeV²
$Q^2= 4$ GeV²
10^4
10^3
10^2
10
1
10^{-5}
10^{-4}
10^{-3}
10^{-2}
10^{-1}
1

This figure "fig1-5.png" is available in "png" format from:

http://arXiv.org/ps/hep-ph/9503266v1

Fig. 5

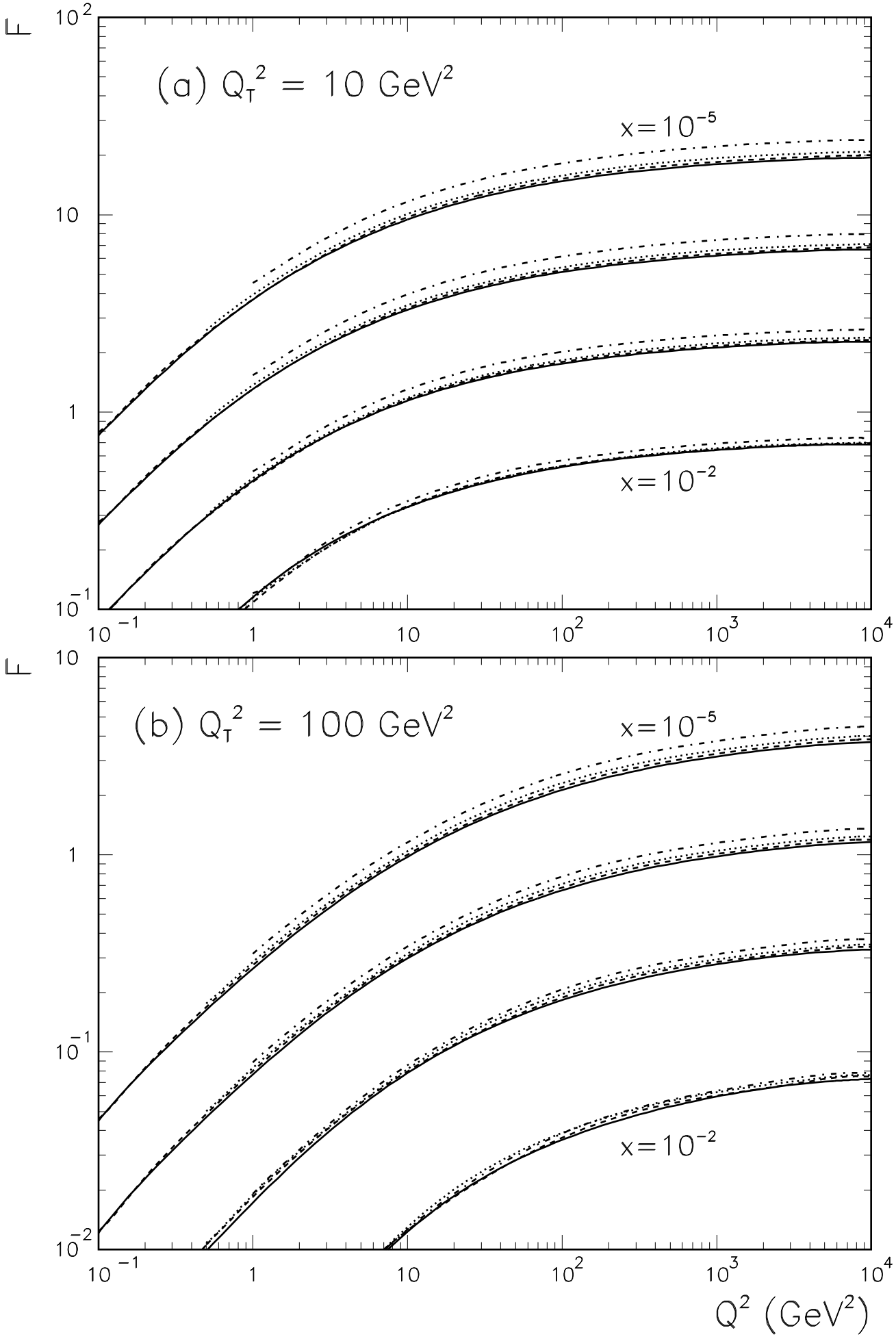
F
(a) Q_T^2 = 10 GeV^2
x=10^{-5}
x=10^{-2}
10^2
10
1
10^{-1}
10^{-1}
1
10
10^2
10^3
10^4
F
(b) Q_T^2 = 100 GeV^2
x=10^{-5}
x=10^{-2}
10
1
10^{-1}
10^{-2}
10^{-1}
1
10
10^2
10^3
10^4
Q^2 (GeV^2)

This figure "fig1-6.png" is available in "png" format from:

http://arXiv.org/ps/hep-ph/9503266v1

Fig. 6

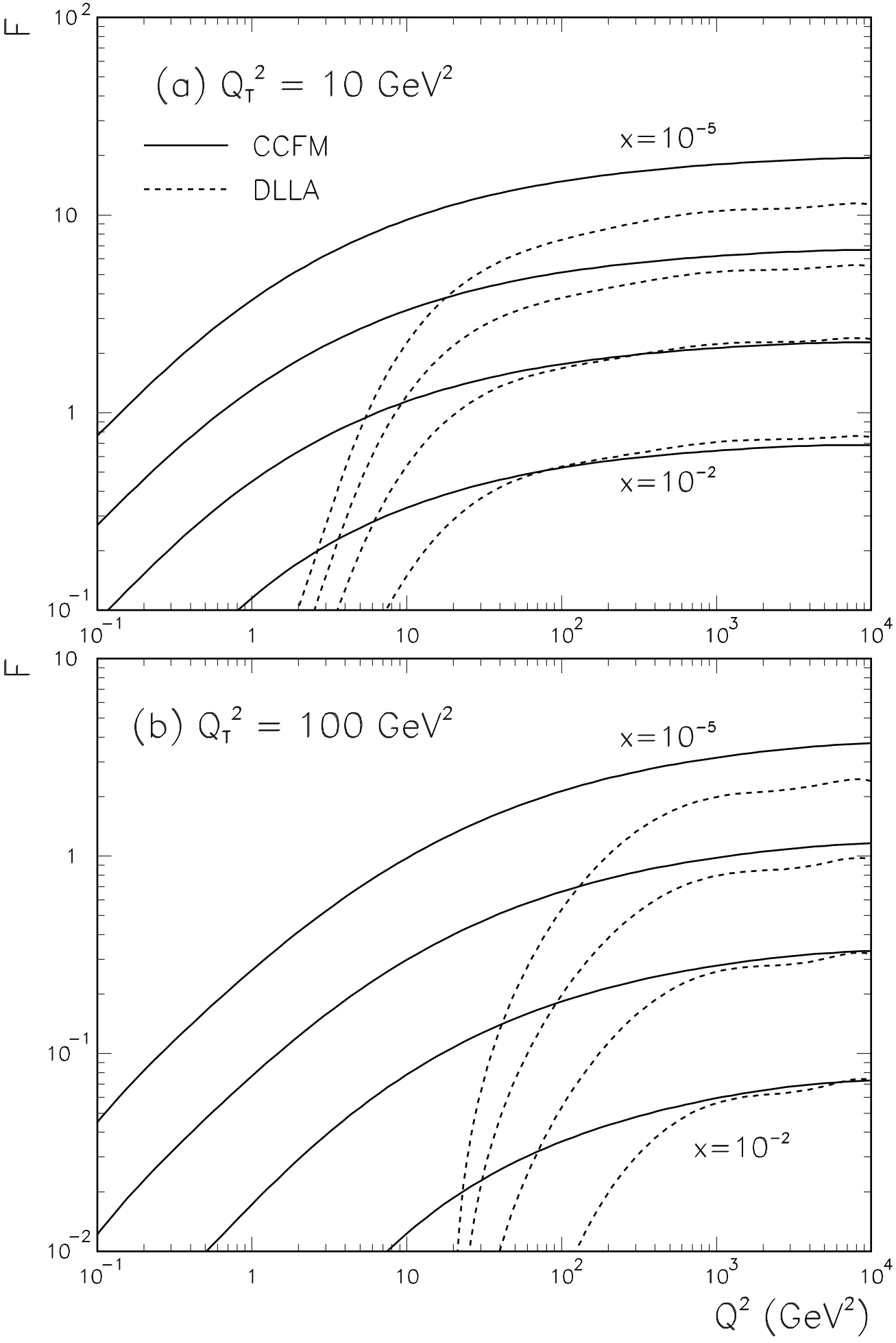
(a) Q_T^2 = 10 GeV^2
CCFM
DLLA
x=10^{-5}
x=10^{-2}
F
10^2
10
1
10^{-1}
10^{-1}
1
10
10^2
10^3
10^4
(b) Q_T^2 = 100 GeV^2
x=10^{-5}
x=10^{-2}
F
10
1
10^{-1}
10^{-2}
10^{-1}
1
10
10^2
10^3
10^4
Q^2 (GeV^2)

This figure "fig1-7.png" is available in "png" format from:

http://arXiv.org/ps/hep-ph/9503266v1

Fig. 7

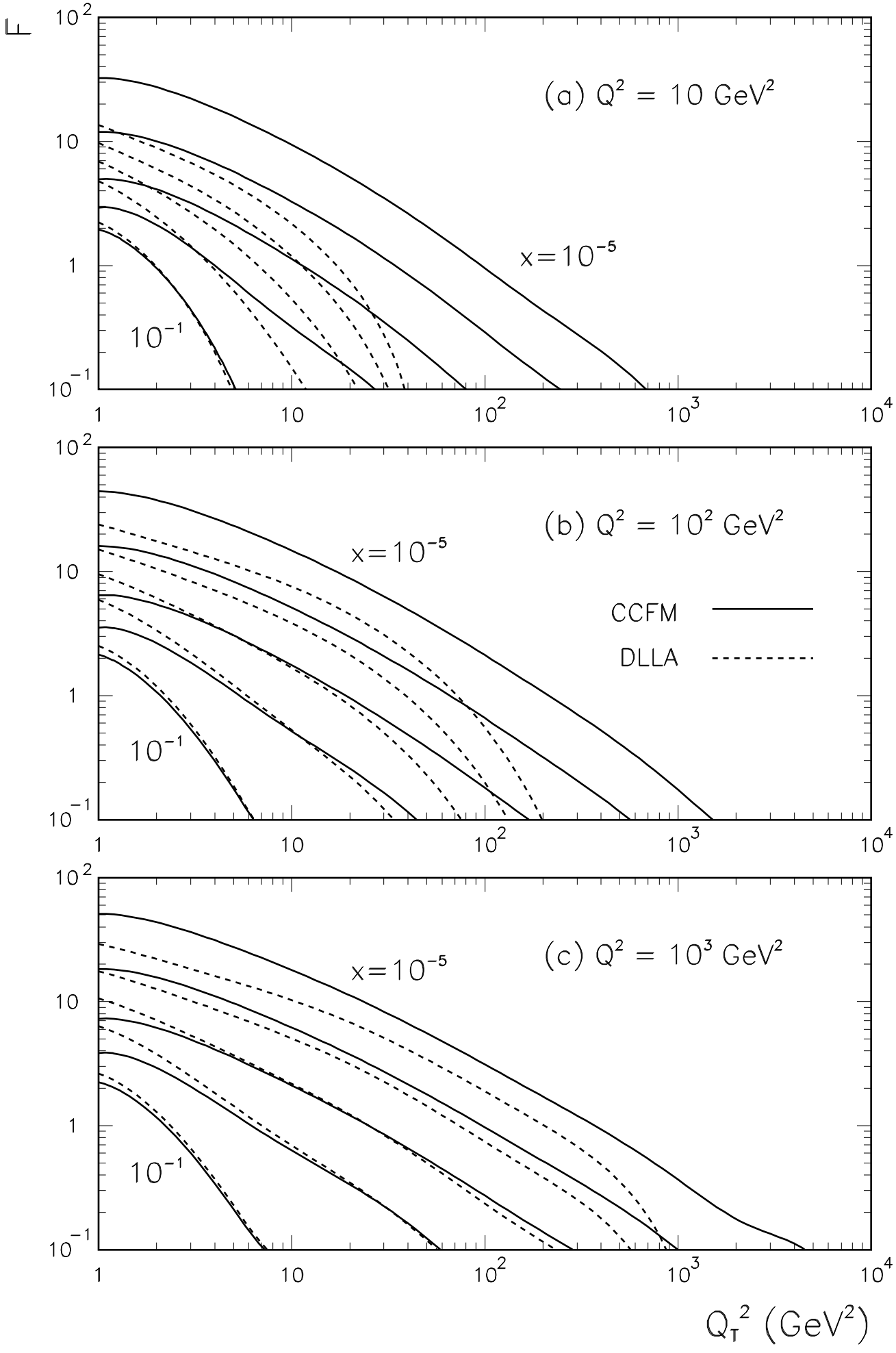
F
(a) Q^2 = 10 GeV^2
x=10^{-5}
10^{-1}
(b) Q^2 = 10^2 GeV^2
x=10^{-5}
10^{-1}
CCFM
DLLA
(c) Q^2 = 10^3 GeV^2
x=10^{-5}
10^{-1}
Q_T^2 (GeV^2)

This figure "fig1-8.png" is available in "png" format from:

http://arXiv.org/ps/hep-ph/9503266v1

Fig. 8

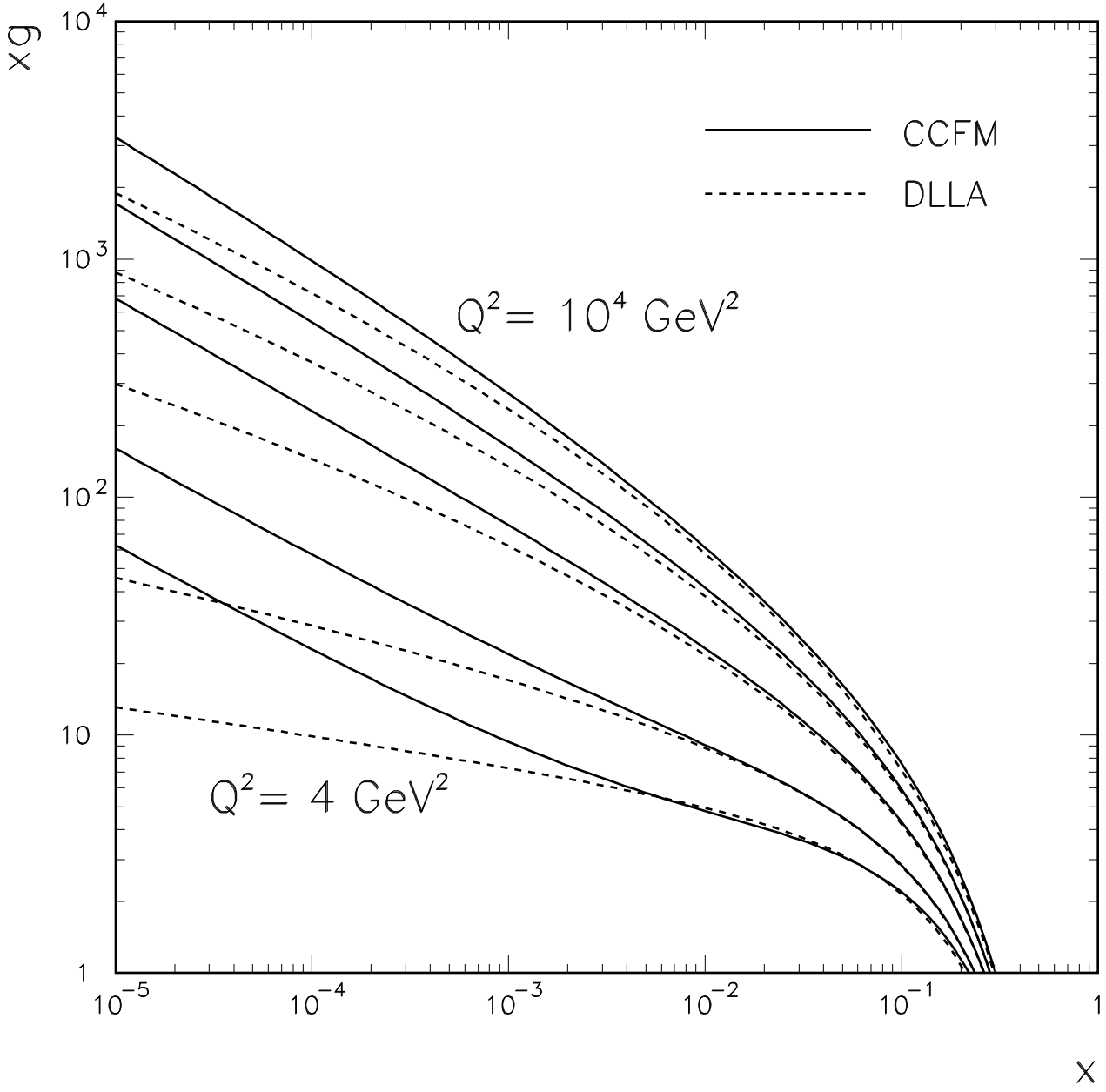
xg
10^4
10^3
10^2
10
1
10^{-5}
10^{-4}
10^{-3}
10^{-2}
10^{-1}
1
X
CCFM
DLLA
$Q^2 = 10^4$ GeV^2
$Q^2 = 4$ GeV^2

Fig. 9

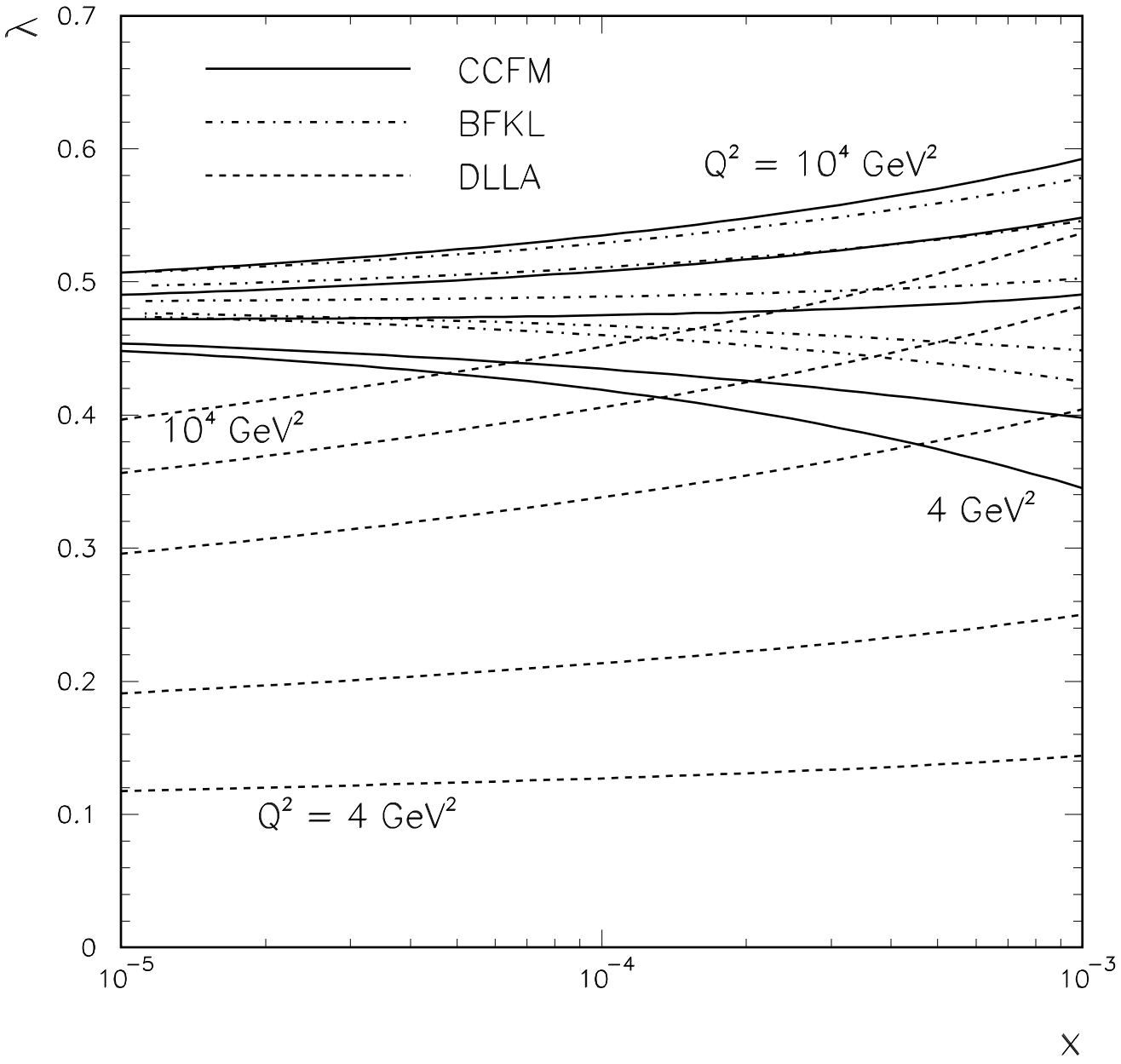
λ
0.7
0.6
0.5
0.4
0.3
0.2
0.1
0
CCFM
BFKL
DLLA
Q² = 10⁴ GeV²
10⁴ GeV²
4 GeV²
Q² = 4 GeV²
10⁻⁵
10⁻⁴
10⁻³
X

Fig. 10

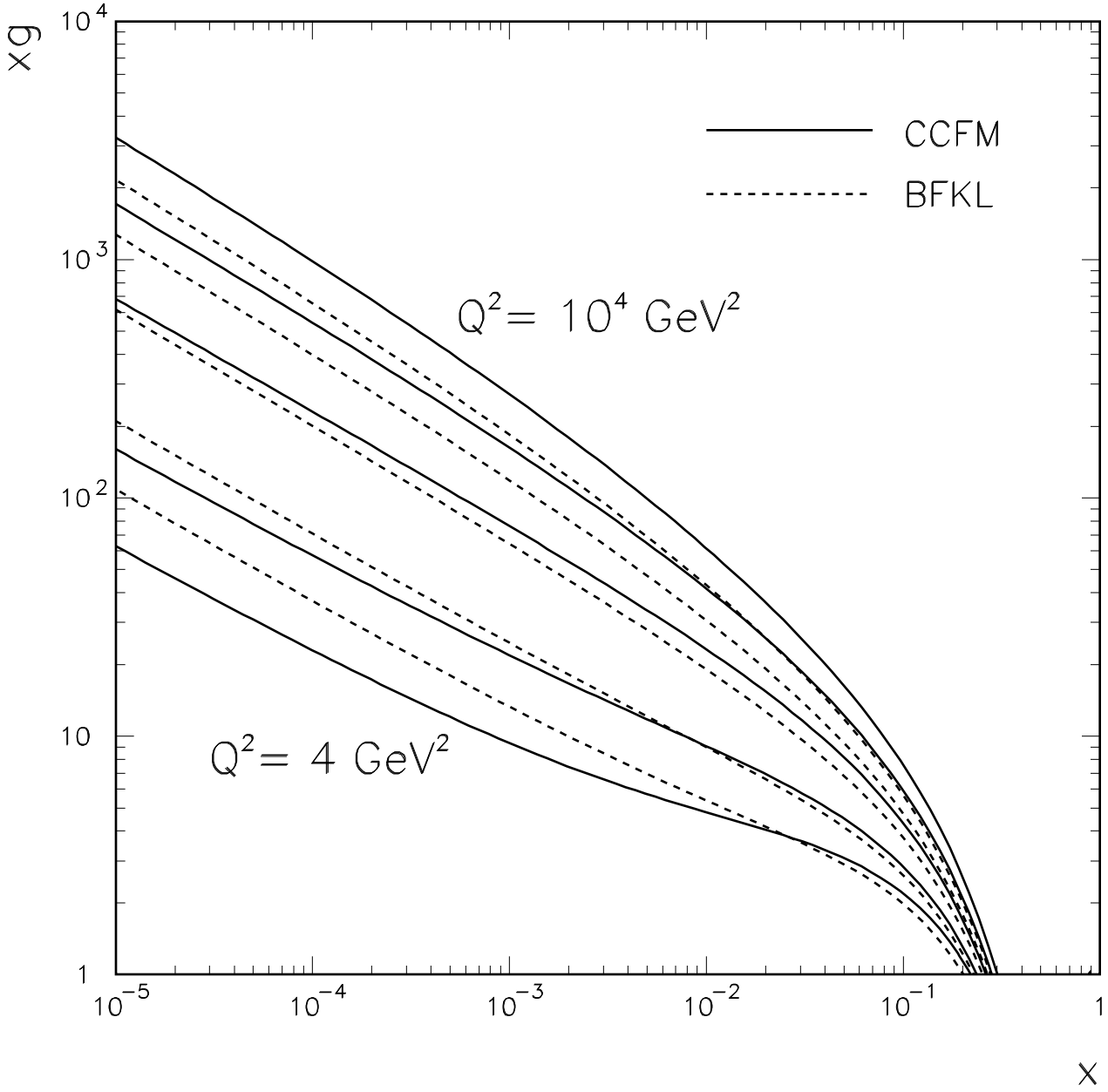
xg
10^4
10^3
10^2
10
1
10^{-5}
10^{-4}
10^{-3}
10^{-2}
10^{-1}
1
x
CCFM
BFKL
$Q^2 = 10^4$ GeV^2
$Q^2 = 4$ GeV^2

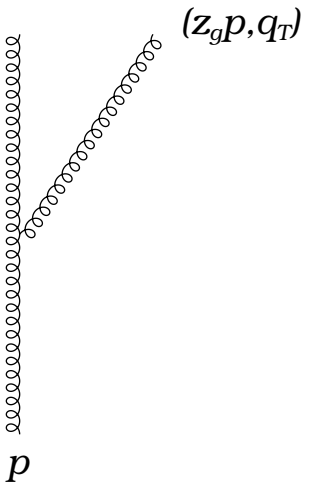

Fig. 1

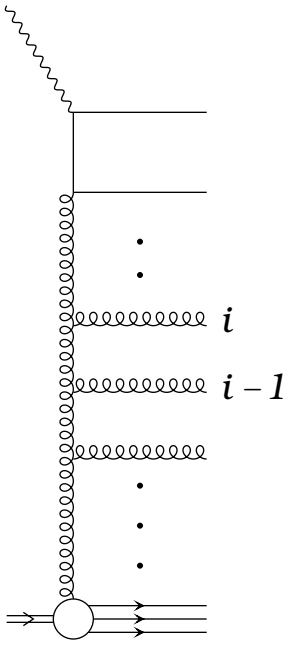

Fig. 2

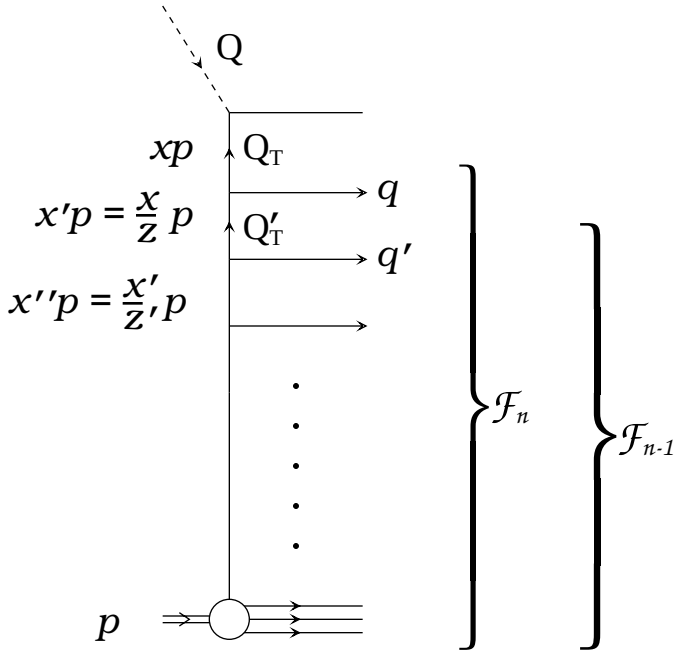

Fig. 3